

A pulsed atomic soliton laser

L. D. Carr

JILA, National Institute for Standards and Technology and University of Colorado, Boulder, CO 80309-0440

J. Brand

*Max Planck Institute for the Physics of Complex Systems,
Nöthnitzer Straße 38, 01187 Dresden, Germany*

(Dated: November 9, 2018)

It is shown that simultaneously changing the scattering length of an elongated, harmonically trapped Bose-Einstein condensate from positive to negative and inverting the axial portion of the trap, so that it becomes expulsive, results in a train of self-coherent solitonic pulses. Each pulse is itself a non-dispersive attractive Bose-Einstein condensate that rapidly self-cools. The axial trap functions as a waveguide. The solitons can be made robustly stable with the right choice of trap geometry, number of atoms, and interaction strength. Theoretical and numerical evidence suggests that such a pulsed atomic soliton laser can be made in present experiments.

PACS numbers: 05.45.Yv, 03.75.-b, 03.75.Fi

I. INTRODUCTION

Solitons have applications in a wide variety of physical contexts, ranging from water waves to photonic crystals [1, 2, 3]. For example, they have been used in transatlantic communications systems, where the need for expensive amplifiers mid-line in fiber optic cables that run over long distances is reduced or eliminated. By virtue of their many uses, as well as their mathematical beauty, solitons are a continuing subject of vigorous research (see, for example, [4, 5]). In particular, they have proven highly useful in laser applications [3]. Non-linear materials are used to cause high-intensity coherent light waves emitted by lasers to self-focus into stable non-dispersive pulses.

Bose-Einstein condensates (BEC's) are coherent matter waves in analogy to coherent light waves. BEC's are usually generated as a standing wave in a trap which functions as a cavity. When outcoupled from the trap, a BEC can provide a highly brilliant source of coherent matter-wave radiation, and as such is commonly called an *atom laser*. The challenge in making a BEC into a useful atom laser is in the outcoupling [6, 7]. To this end, many experimental methods have been developed. Anderson and Kasevich [8] tilted a BEC trapped in a periodic potential created by a standing light wave. The gravitational field induced by the tilt caused the condensate to tunnel through the wells and interfere coherently, thereby creating a pulsed atom laser. Bloch et al. [9] used an external laser to change the spin state of atoms in two locations in a harmonic magnetic trap. The condensed atoms then spilled out, again due to gravitational effects; the two separate outcouplings allowed them to make the first clear demonstration of coherence along the whole length of the beam. Many experiments and proposals have followed. All of these atom lasers were studied in the context of repulsive BEC's. Repulsive BEC's naturally disperse in all directions; even axial confinement in

a waveguide cannot prevent spreading in the direction of propagation.

The unique contribution of the present study is to show how an *attractive* BEC can be made into an atom laser. A repulsive BEC fractures near conducting surfaces [10], spreads out, and in general is easily excited. In contrast, an attractive BEC, so long as it is axially confined and the experimental parameters are chosen properly, can be made into a pulsed atomic soliton laser which is robustly stable against all of these effects. Moreover, attractive BEC's in this form may be superior to repulsive BEC's in applications to atom chips [11, 12] and interferometry [13]. For instance, in the “nevatron”, a BEC storage ring, the wave packet of repulsive Bose-condensed atoms circulates a few times before spreading out and decohering [14]. This effect is accentuated by superconducting wires which lie transverse to the direction of propagation. A bright soliton would not only be non-dispersive, but, even if excited by the passage over the jump in potential created by the wire, would quickly self-cool by emitting a small fraction of its atoms, typically less than a fraction of a percent [15, 16]. It could therefore circulate indefinitely, subject to three-body recombination rates and other effects beyond those of the mean field [17].

In the following, we explain how to create such a pulsed atomic soliton laser. Bright matter-wave solitons have been created, both singly [18] and in trains [19]. It is shown that a combination of the experimental techniques of Refs. [18] and [19], together with the right choice of parameters, suffices to create a pulsed atomic soliton laser from an attractive BEC. After presenting the basic method in Sec. II, we illustrate its viability via three-dimensional simulations in Sec. III. Then, in Secs. IV and V, the stability criteria and important dynamical features of the pulsed atomic soliton laser are explained in detail. In Sec. VI, the simulations are discussed in light of the results of Secs. IV and V. Finally, in Sec. VII we conclude.

II. BASIC METHOD

The 3D Nonlinear Schrödinger equation (NLS) or Gross-Pitaevskii equation which describes the mean field of the BEC is written as [17]

$$\left[-\frac{\hbar^2}{2m}\nabla^2 + gN|\Psi|^2 + V(\vec{r}) \right] \Psi = i\hbar\partial_t\Psi, \quad (1)$$

where

$$V(\vec{r}) \equiv \frac{1}{2}m(\omega_\rho^2\rho^2 + \omega_z^2z^2), \quad (2)$$

$g \equiv 4\pi\hbar^2a/m$, a is the s -wave scattering length, m is the atomic mass, N is the number of condensed atoms, the condensate order parameter $\Psi = \Psi(\vec{r}, t)$ has been normalized to one, and axisymmetric harmonic confinement has been assumed. Note that for negative scattering length, or attractive nonlinearity, solutions are liable to collapse in certain parameter regimes [5, 20], as shall be discussed below. With the exception of Sec. VB, where the decoherence time between pulses is estimated, it is assumed that the BEC is described by Eq. (1).

The basic method for creating the pulsed atomic soliton laser is as follows.

1. A repulsive BEC is created in an elongated harmonic trap such that $\omega_z \ll \omega_\rho$.
2. The scattering length is made small and negative via the now well-established experimental technique of using a magnetically induced Feshbach resonance [18, 19, 21, 22].
3. Simultaneously, the axial potential is changed from small and attractive (ω_z real) to small and expulsive (ω_z imaginary) [16, 18, 23].
4. The condensate becomes modulationally unstable to spatial pulse formation. This instability is non-dissipative. The pulses are seeded by self-interference of the order parameter, as we have elsewhere described [24]. The initial growth rate of the modulational instability can be calculated via linear perturbation theory [25].
5. The ensuing solitonic pulses are subject to *primary collapse* in two or three dimensions, as well as *secondary collapse* due to soliton-soliton interactions [24]. Furthermore, if they are too long in the z -direction they can be torn apart by the force of the expulsive harmonic potential [16]. With the right choice of parameters, these effects can be avoided and the solitonic pulses made robustly stable, as shall be described in Sec. IV.
6. The solitons continue to accelerate. Their relative spacing increases as $\Delta z \propto \exp(|\omega_z|t)$.

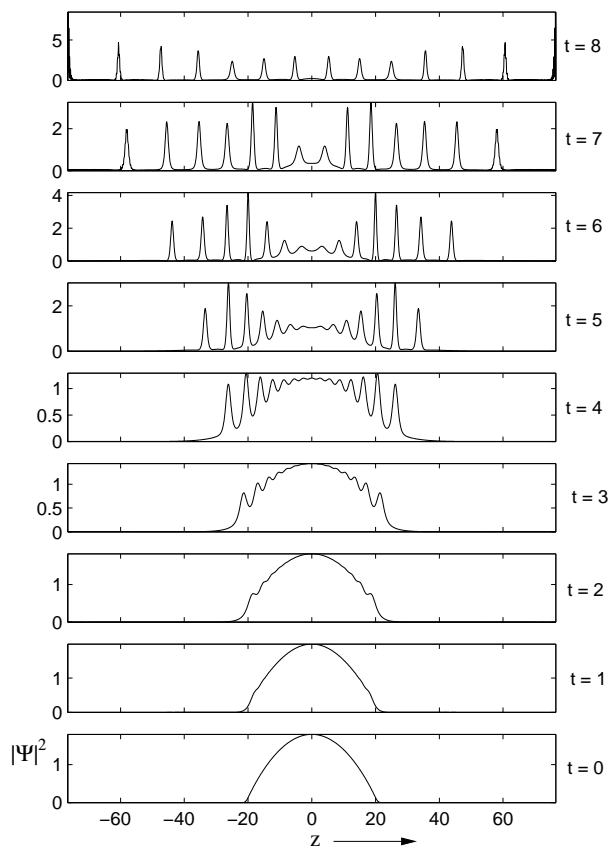


FIG. 1: Shown is the evolution of an attractive Bose-Einstein condensate into a pulsed atomic soliton laser. Time slices of the line density in z are shown for $x, y = 0$. Modulational instability of the initial density profile is seeded by self-interference of the order parameter, so that solitons form first at the cloud edges and later towards the center. The latest, top panel, shows that a well-separated set of stable solitonic pulses are produced. Note that, for $N = 10^4$ atoms, $a = -3a_0$, and a trap geometry of $\omega_\rho = 2\pi \times 2.44$ kHz, $\omega_z = 2\pi i \times 2.26$ Hz, the time units are scaled to 22 ms and the spatial units to 10 μm .

7. The expulsive harmonic potential can eventually be coupled to a linear or even a flat potential for applications. We do not discuss the various possibilities here.

An important point is that even if the coupling is not smooth, each soliton responds to perturbation by a shift in its phase and by emitting a small number of atoms, typically a fraction of a percent of the total number in the soliton. Insofar as an excited BEC described by the NLS models a condensate plus thermal field [26, 27], where the “condensate” is a stationary solution, one may term this process *self-cooling*. As each soliton is itself a BEC, this model can be applied to each pulse separately. Self-cooling to $T = 0$ in an expulsive harmonic potential occurs exponentially, with the density fluctuations at the center of each solitonic pulse falling off as $\exp(-|\omega_z|t)$ [16].

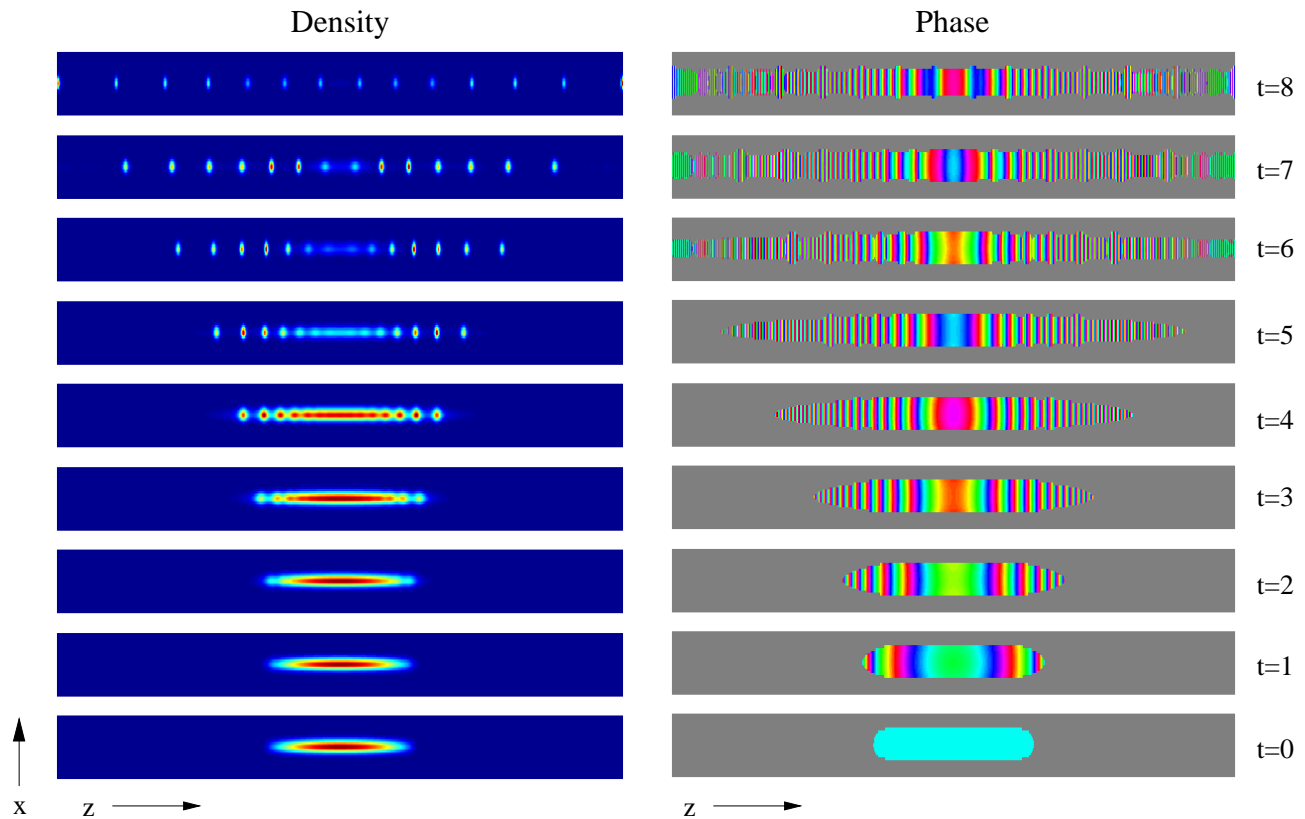


FIG. 2: Shown are the evolution of the density and phase along a two dimensional cut at $y = 0$ for the simulation of Fig. 1. A set of well-defined solitonic pulses is evident in the latest (top) panel. The strong variations in the phase at late times is due to the high momentum of the solitons caused by the expulsive harmonic potential. Note that the phase is shown on the color circle, *i.e.*, modulo 2π , while the density is in arbitrary relative units rescaled for each plot. The aspect ratio of the plots showing a region of 0.822 by 153 length units was changed for visualization; length and time units are the same as in Fig. 1.

One may ask what this schemata has in common with the operation of a normal, light-wave laser. Insofar as the initial condition is an excited mode of the harmonic trap plus mean field potential, and the ensuing pulse train is a much lower energy mode, this situation has a certain analogy with population inversion. As was mentioned in the introduction, the initial trapping potential may be considered as a cavity, with the outcoupling provided by the sudden change to an expulsive trapping potential in the axial direction. However, the emission of solitonic pulses is not stimulated, as strictly required for the use of the acronym LASER (light amplification by stimulated emission of radiation), but rather spontaneous. The analogy of the proposed scheme to the operation of a laser is therefore rather in the output than in the detailed mechanism of its operation: one produces a train of non-phase-locked self-coherent pulses.

III. PULSED ATOMIC SOLITON LASER DYNAMICS: PROOF OF PRINCIPLE SIMULATIONS

Three dimensional simulations of Eq. (1) were performed, with parameters which satisfied the criteria given in Sec. IV. Cylindrical symmetry was assumed in order to make computations with a large grid size possible (2048×16) [28]. The initial profile was obtained by imaginary time relaxation. This resulted in a Thomas-Fermi-like profile in the z direction (see Eq. (26) below and [17]), and a nearly Gaussian one in x and y . A trap of aspect ratio $\omega_\rho/\omega_{z0} = (\ell_{z0}/\ell_\rho)^2 = 538$ and nonlinearity parameter $a_{s0}N/\ell_{z0} = 1.02$ was used to produce the initial state, where ω_{z0} , ℓ_{z0} and a_{s0} all refer to these initial conditions, and $\ell_i \equiv \sqrt{\hbar/(m\omega_i)}$.

At $t = 0$, the longitudinal trapping frequency ω_{z0} was changed to a weak expulsive harmonic potential with $\omega_z = 0.5i\omega_{z0}$, and the nonlinearity was switched from repulsive to attractive, with $-aN/\ell_{z0} = 0.0854 = 0.00368 \ell_{z0}/\ell_\rho$. As attractive BEC's can collapse in three dimensions, this is an important point in the choice of parameters. The length unit in the simulations is $u = 0.56\ell_{z0}$ and the time unit $\tau = 2mu^2/\hbar$. To com-

pare with experimental parameters, one must choose the number of particles and a scaling factor, e. g. $u = 10\mu\text{m}$ and $N = 10^4$, which corresponds to $\tau = 22\text{ms}$, $\omega_{z0} = 2\pi \times 4.53\text{Hz}$, $\omega_z = 2\pi i \times 2.26\text{Hz}$, and $\omega_\rho = 2\pi \times 2.44\text{kHz}$ with a scattering length of $a = -3a_0$.

Figures 1 and 2 illustrate the evolution of the density and phase of the condensate in time slices through the x - z plane for $y = 0$ with the above described initial state and parameters. Several observations may be made based on the figures. Firstly, the final number of solitons is 14. Secondly, they are stable against collapse and, once formed, do not subsequently interact over the lifetime of the simulation. Thirdly, solitons form first at the edges of the cloud, then later towards the center, as was also observed in a simplified model in our previous work [24]. We note that no white or colored noise was added to this simulation. The reasoning behind our choice of parameters will be discussed in Sec. IV, while the details of the simulation itself will be interpreted in Secs. V and VI.

IV. STABILITY CRITERIA

In order that the pulsed atomic soliton laser be robustly stable over the lifetime of an experiment, a set of criteria must be satisfied. These criteria are detailed in the following subsections. Note that in the below considerations we are interested in stability for experimental purposes, not mathematical stability to infinite time.

A. Two-dimensional primary collapse

Two-dimensional transverse primary collapse must be avoided. In the case of strongly anisotropic axisymmetric confinement, one may adiabatically separate the slow longitudinal from the fast transverse degrees of freedom. The adiabatically varying transverse state obeys a 2D NLS which shows an instability towards collapse. The criterion for stability found by numerical integration of the 2D NLS is

$$-8\pi a n_{1D}(z, t) < \eta_c^{2D} = 11.7 \dots, \quad (3)$$

where $n_{1D}(z, t)$ is the local axial line density of the condensate [29]. If adiabaticity is violated, collapse can also happen at weaker nonlinearity due to transverse oscillations on a time scale π/ω_ρ [30]. When the longitudinal dynamics is significantly slower than this time scale, the adiabatic separation of scales is valid. If, additionally, the transverse nonlinearity is weak, *i.e.*, $|8\pi a n_{1D}(z, t)| \ll 1$, the longitudinal equation reduces to the quasi-1D NLS

$$\left[-\frac{\hbar^2}{2m} \partial_z^2 + g_{1D} N |\psi|^2 + \frac{1}{2} m \omega_z^2 z^2 \right] \psi = i \hbar \partial_t \psi, \quad (4)$$

where $g_{1D} \equiv 2a\omega_\rho\hbar$ is the renormalized quasi-1D coupling constant [16], provided $\ell_\rho \gg |a|$ [31], with $\ell_\rho \equiv \sqrt{\hbar/(m\omega_\rho)}$.

B. Three-dimensional primary collapse

Three-dimensional primary collapse of the individual solitonic pulses in the atom laser must be avoided. The static condition based on imaginary time relaxation of Eq. (1) is [16]

$$-\frac{N_{\text{ais}} a}{\ell_\rho} < \eta_c^{3D} = 0.627 \dots, \quad (5)$$

where $N_{\text{ais}} \sim N/N_s$ is the number of atoms in a soliton, with N_s the number of solitons (see Sec. VI below). Replacing the $<$ sign with a \ll sign ensures stability for an excited soliton. Note that the value of η_c^{3D} can vary slightly as the anisotropy of the trap changes [16, 32]. However, 3D collapse is essentially an isotropic phenomenon, with the trap simply setting the initial conditions [33].

C. Explosion of individual solitonic pulses

The soliton can become unstable when the expulsive potential overcomes the balance between the mean field energy and kinetic energy necessary for the soliton's existence and destroys it by tearing it in two [16]. We term this kind of possible instability *explosion*. In order to avoid explosion, the geometry must be chosen so that $\ell_z \gg \ell_{\text{sol}}$, where $\ell_z \equiv \sqrt{\hbar/m|\omega_z|}$. The soliton length $\ell_{\text{sol}} \sim \xi$, where ξ is the healing length, can be determined as follows. Taking the form of the soliton as the well-known solution in one dimension for a constant potential (see [16] and references therein)

$$\psi(z, t) = \frac{1}{\sqrt{2\ell_z}} \text{sech}\left(\frac{z}{\ell_z}\right) e^{-i\mu t}, \quad (6)$$

and substituting into Eq. (4) while temporarily neglecting the trapping potential, one obtains $\ell_z = 2\hbar^2/(m|g_{1D}|N_{\text{ais}})$. Then

$$\ell_{\text{sol}} \simeq \frac{\ell_\rho}{|a|N_{\text{ais}}} \ell_\rho, \quad (7)$$

where the wavefunction has been renormalized to account for the division of N total atoms into N_{ais} atoms in any given soliton. Note that the prefactor is the inverse of the ratio which must be small to avoid 3D collapse, as given by Eq. (5) in the preceding subsection.

A variational analysis based on a hyperbolic secant *ansatz* and Eq. (4) with the trapping potential gives a more precise condition to avoid explosion as [16]

$$\frac{\ell_z}{\ell_{\text{sol}}} > \left(\frac{2^6 \pi^4}{3^3}\right)^{1/4} = 2.20 \dots \quad (8)$$

In the quasi-1D regime far from collapse, such a variational analysis typically gives estimates to better than 1%. As in Eq. (5), the $>$ sign can be replaced with a \gg sign to ensure stability for an excited soliton.

D. Soliton–soliton interaction and secondary collapse

The harmonic potential must be sufficiently strong so as to prevent secondary collapse caused by soliton–soliton interaction. If two solitons overlap coherently they can violate the stability criterion of Eq. (5), due to the doubling of the number of atoms. Even if, due to decoherence during soliton propagation (see Sec. VB below), their relative phase is not defined prior to interaction, upon interacting they develop a well-defined relative phase [34].

In order to treat soliton motion in a slowly varying potential, as defined explicitly by the condition of Eq. (8), one may suppose a separation of scales, as may be formally defined by a multiscale analysis (see, for example, Ref. [35]). In this case an approximate equation of motion for the relative soliton parameters is given by [36, 37]

$$\begin{aligned}\ddot{\phi} &= \frac{8\hbar^2\kappa^4}{m^2} \sin(\phi) \exp(-\kappa r) \\ \ddot{r} &= -\frac{8\hbar^2\kappa^3}{m^2} \cos(\phi) \exp(-\kappa r) - \omega_z^2 r,\end{aligned}\quad (9)$$

where

$$\kappa \equiv -Ng_{1D}m/\hbar^2, \quad (10)$$

$\phi \equiv \phi_1 - \phi_2$ is the relative phase, $r \equiv |z_1 - z_2|$ is the relative position, with the two solitons indicated by indices 1, 2, and motion according to Eq. (4) has been assumed. Equation (9) describes a separated soliton pair, *i.e.*, the motion outside the interaction region: it breaks down as they overlap fully. With respect to Refs. [36, 37], we have here added the physical units relevant for the BEC and the expulsive harmonic potential.

To prevent soliton–soliton interaction it is necessary that the potential due to the expulsive harmonic potential be much stronger than that due to the attraction between solitons. Taking $\phi(t) \equiv \dot{\phi}(t) \equiv 0$, which assumes that the solitons are initially in-phase and have the same amplitude, the two potentials are given by

$$V_{\text{ho}} = \frac{1}{2}m\omega_z^2 r^2, \quad (11)$$

$$V_{\text{sol}} = 8\frac{\hbar^2\kappa^2}{m^2} \exp(-\kappa r). \quad (12)$$

In case the solitons are not initially in phase or do not have the same amplitude, the criterion will only be less stringent. It is therefore sufficient that

$$\left(\frac{\ell_\rho}{\ell_z}\right)^4 \left(\frac{\ell_\rho}{|a|N_{\text{ais}}}\right)^4 \frac{N_{\text{ais}}^2}{N_s^2} \gg \frac{2^6}{\pi^2} \exp(-8\pi N_s/N_{\text{ais}}). \quad (13)$$

Here the first factor in parentheses is the trap aspect ratio while the second factor is again the inverse of the 3D collapse criterion of Eq. (5).

The question then arises as to whether or not the trap can be made sufficiently strong so as to prevent soliton

interactions, as required by Eq. (13), and at the same time sufficiently weak so as not to cause the individual solitons to explode, as required by Eq. (8). Putting these two criteria together, one finds

$$\chi^{-2} \gg \frac{3^3}{\pi^6} \exp(-8\pi\chi), \quad (14)$$

where $\chi \equiv N_s/N_{\text{ais}}$. This relation is always fulfilled, showing that the two criteria are compatible.

V. DYNAMICAL FEATURES

There are two aspects of the dynamics which are necessary to discuss in detail. Firstly, there has been some debate as to the mechanism of soliton formation. In Sec. VA, it is argued that both dynamically generated fluctuations from self-interference of the order parameter [24] and noise due to thermal fluctuations [38] or fluctuations in the trapping potential [39], as seen experimentally close to surfaces [40], cause the BEC to become modulationally unstable on approximately the same time scale. Secondly, outside of the mean field model encapsulated in the NLS, one may ask how long it takes for the relative phase of solitonic pulses in the atom laser to randomize, or decohere. In Sec. VB, an estimate of this time scale is made.

Two issues which we do not discuss in any detail are quantum evaporation and center of mass motion. The former is studied in detail in Ref. [16], where it is shown that matter-wave bright solitons in an expulsive potential evaporate and eventually explode. However, the tunneling rates are so small in the parameter regimes of interest to the present work so as to be unimportant. With regards to the latter, in a harmonic potential the center of mass and relative degrees of freedom are entirely decoupled, so that we need only consider the relative soliton motion [41]. The center of mass motion is, in any case, trivial: $z_{\text{com}}(t) = z_{\text{com}}(0) \exp(i\omega_z t)$ in the quasi-1D regime.

A. Seeding of modulational instability: self-interference vs. noise

In order to understand the mechanism of modulational instability for a non-uniform initial density profile and in the presence of a non-constant potential, it is necessary to briefly review modulational instability in the uniform case, which is well known from fiber optics [25]. A linear response analysis reveals that, for attractive nonlinearity, a small sinusoidal modulation of a uniform state ψ_0 with wavenumber k grows with time at a rate γ given by

$$\gamma^2 = -\frac{\hbar^2}{4m^2} \left[k^2 - \frac{2m|g_{1D}|n_{1D}}{\hbar^2} \right]^2 + \frac{n_{1D}^2|g_{1D}|^2}{\hbar^2}. \quad (15)$$

The maximum growth rate

$$\gamma_{\text{mg}} = 2\omega_\rho |a| n_{1D} \quad (16)$$

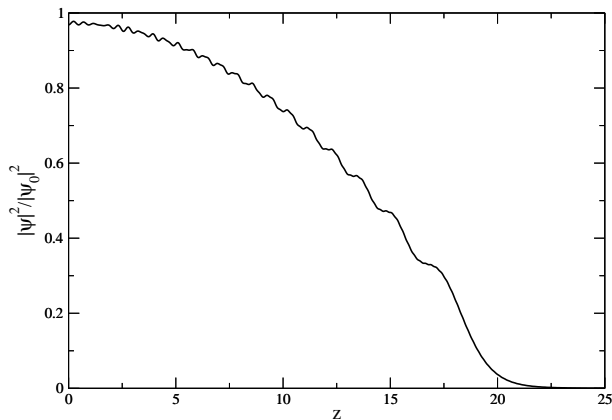


FIG. 3: Shown are the self-interference fringes of the order parameter which seed modulational instability, according to the Feynman propagator for a harmonic oscillator. The initial density profile was Thomas-Fermi; shown is the ratio of the density 66 ms later to the original density. Since the wavelength of the instability must be on the order of $2\pi\xi$, where ξ is the healing length, solitons form first on the edges of the cloud, due to the early long wavelength fringes in this region. At later times the wavelength of the fringes in the center also becomes longer. Shown is the linear equivalent of the panel depicting $t = 3$ in the full simulation of the 3D Gross-Pitaevskii equation illustrated in Figs. 1 and 2; all parameters are the same as the simulation, with length units scaled to 10 μm .

is obtained at wavenumber

$$k_{\text{mg}} = 1/\xi, \quad \xi \equiv \ell_\rho / \sqrt{4|a|n_{1\text{D}}}, \quad (17)$$

where ξ is the effective 1D healing length of the condensate [42] and $n_{1\text{D}} = N|\psi_0|^2 = N/L$ is the line density. Growth occurs only if $\gamma^2 > 0$, which implies $0 < k < k_{\text{max}} = \sqrt{2}k_{\text{mg}}$. This means that nonlinear focusing can only be seeded by modulations of sufficiently long wavelength and is fastest at the length scale of $2\pi\xi$.

For a non-uniform initial density profile, there are two ways in which modulational instability can occur. Either it can be seeded by noise, or it can be seeded by fringes caused by self-interference of the order parameter. The time scale of the two mechanisms turns out to be approximately the same, as shall be shown in the following. A similar number of solitons results, but in the former case they form first in the higher density regions (typically the center, for a Thomas-Fermi-like initial profile [17]), while in the latter case they form first at the edges, as illustrated in Figs. 1 and 2 and explained in our previous work [24].

Consider first the case of self-interference. An analysis based on the Feynman propagator for the *linear* Schrödinger equation in a harmonic potential shows that self-interference, or diffraction, of the order parameter leads to fringes which have the correct length scale to seed modulational instability [24]. Our findings of Ref. [24] were supported later by Kamchatnov *et al.*, who used Whitham theory to describe the nonlinear evolution of

the diffraction pattern of a rectangular initial density profile [43]. Our previous analysis was performed for a rectangular initial density profile in order to obtain closed form analytic results [24]. The Feynman propagator is defined by

$$\psi(z, t) = \int dz' G(z, t; z', 0) \psi(z', 0). \quad (18)$$

For a harmonic oscillator, the propagator is

$$G = \frac{\exp\{i(z^2 - 2zz'/\cos\tau + z'^2)/(2\ell_z^2 \tan\tau)\}}{\ell_z \sqrt{2\pi i |\sin\tau|}}, \quad (19)$$

where

$$\tau \equiv \omega_z t. \quad (20)$$

In the limit $\tau \ll 1$, and for a rectangular initial density profile, the result of the integration of Eq. (18) can be Taylor expanded as

$$\begin{aligned} |\psi(z, t)|^2 / |\psi(z, 0)|^2 \simeq 1 + \\ \sqrt{\frac{8\ell_z^2 \tau}{\pi}} \left[\frac{\sin(k_+ z + \delta - \frac{\pi}{4}) \sin(k_- z + \delta - \frac{\pi}{4})}{L + 2z} \frac{1}{L - 2z} \right] + \\ \frac{4\ell_z^2 \tau}{\pi} \left\{ \frac{L^2 + 4z^2}{(L + 2z)^2 (L - 2z)^2} + \frac{\cos[(k_+ - k_-)z]}{(L + 2z)(L - 2z)} \right\}, \quad (21) \end{aligned}$$

$$k_\pm \equiv \frac{\sec(\tau)z \pm L}{2\ell_z^2 \sin(\tau)}, \quad \delta \equiv \frac{L^2 \cot(\tau)}{8\ell_z^2}, \quad |z| < \frac{L}{2}. \quad (22)$$

To linear order in τ , the trapping frequency drops out of the equations, since $\ell_z^2 \tau = \hbar t/m$. Equations (21) and (22) describe the formation of fringes. Note that, according to the argument of the exponential in the Feynman propagator (19), at the quarter period the wavefunction is Fourier transformed with respect to its initial state. Therefore any initial wavefunction excepting a Gaussian must develop fringes. A time scale can be estimated from these prefactors in the expansion of Eq. (21). Fringes appear at a length scale ℓ_{fringe} at time

$$t \simeq \frac{m}{\hbar} \ell_{\text{fringe}}^2. \quad (23)$$

This argument can also be made simply by the units in the problem. The length scale at which modulational instability is maximally probable is $\ell_{\text{fringe}} = 2\pi\xi$. Therefore, the time scale for fringe formation leading to modulational instability may be estimated as

$$t_{\text{fringe}} \simeq \frac{\pi^2}{2\omega_\rho |a| \bar{n}_{1\text{D}}}, \quad (24)$$

where $\bar{n}_{1\text{D}}$ is the mean linear density and we have taken the mean density as $\bar{n} = \bar{n}_{1\text{D}}/\pi\ell_\rho^2$ in order to calculate the healing length. For the parameters of Sec. III, $t_{\text{interference}} \simeq 41$ ms. This is approximately the correct time scale, as observed in Figs. 1 and 2.

In order to study the problem with a more realistic model than an initially rectangular density profile, the longitudinal variation of the density profile is taken as an inverted parabola. This is characteristic of the Thomas-Fermi limit in a harmonic trap, and is the generic experimental case [17]. At the same time, the transverse wavefunction is taken as a Gaussian, in keeping with the quasi-1D approximation. The density then takes the form

$$|\Psi(\vec{r}, 0)|^2 = |\psi(z, 0)|^2 \frac{1}{\sqrt{\pi}\ell_\rho} \exp\left(-\frac{x^2 + y^2}{\ell_\rho^2}\right) \quad (25)$$

$$|\psi(z, 0)|^2 = \frac{\ell_\rho^2(R^2 - z^2)}{4\ell_z^4|a|}, \quad (26)$$

$$R \equiv \left(\frac{3N|a|\ell_z^4}{\ell_\rho^2}\right)^{1/3} \quad (27)$$

$$\ell_z \equiv \sqrt{\hbar/m|\omega_z|}, \quad (28)$$

where $N|\psi(z)|^2$ is the longitudinal line density, R is the Thomas-Fermi radius, and ℓ_z is the longitudinal oscillator length. The linear development of the wavefunction may be found at any time by numerical integration of Eq. (18). Note that, in this case, ω_z is imaginary for the expulsive harmonic potential. An example relevant to Sec. III is shown in Fig. 3. The longer wavelength fringes are clearly visible near the edges of the cloud, as discussed in our previous work [24]. This leads to soliton formation near the edges of the cloud at early times and in the center at late times. The figure uses the same parameters as the simulations of Sec. III, and may be compared to the fourth panel from the bottom, or $t = 3$, in Figs. 1 and 2.

Consider now the case of modulational instability seeded by noise, rather than interference fringes. There are two kinds of noise. They originate in different physical mechanisms. The first is classical white or coloured noise, which may be induced, for example, by fluctuations in the trapping potential. The second is thermal quantum noise, which corresponds to a thermal distribution of Bogoliubov excitations. One may estimate the relevance of the latter from first principles. The Bogoliubov quasi-particle dispersion relation for a Thomas-Fermi profile is [17]

$$E^{\text{bog}} \equiv \begin{cases} \sqrt{\frac{\hbar^2 k^2}{2m} \left[\frac{\hbar^2 k^2}{2m} + 2gN|\Psi(\vec{r})|^2 \right]} & |r| \leq R \\ \frac{\hbar^2 k^2}{2m} + \frac{m\omega^2 r^2}{2} - \mu_m & |r| > R. \end{cases} \quad (29)$$

Substituting the wavenumber of maximum growth for modulational instability, Eq. (17), into Eq. (29), the resulting energy is

$$E_{\text{mg}}^{\text{bog}} = \sqrt{3}g\bar{n}, \quad (30)$$

where \bar{n} is the mean density which can be estimated from Eq. (25). An experimental situation may, e.g.,

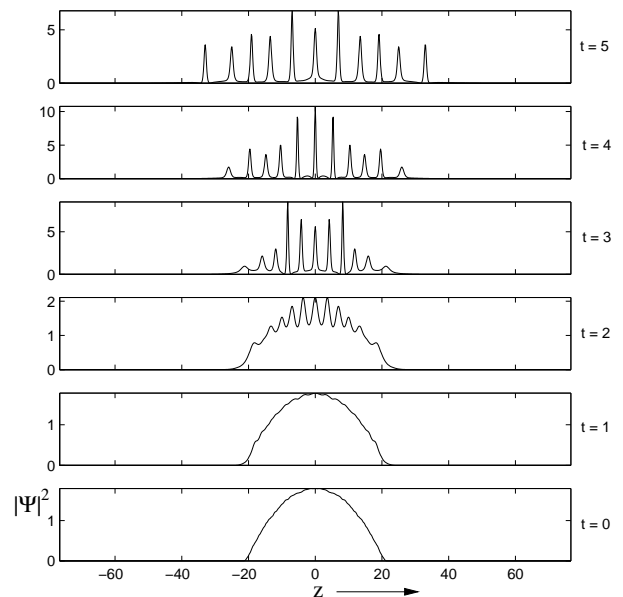


FIG. 4: Shown is the evolution of the density along a one-dimensional cut at $x, y = 0$, with the same parameters as the simulation of Fig. 1 but with the addition of noise, as described in the text. The time scale is shorter than that observed in Fig. 1, and the solitons form first in the center of the cloud, rather than on the outside, but the end result is the same: a set of well-defined solitonic pulses is evident in the latest (top) panel. The length and time units are the same as in Fig. 1.

correspond to an initial temperature of the condensate of $T \simeq T_{\text{BEC}}/2$, with $T_{\text{BEC}} \equiv \hbar\bar{\omega}[N/\zeta(3)]^{1/3}$ and $\bar{\omega} \equiv (\omega_\rho^2\omega_{z0})^{1/3}$. In this case, one can estimate the probability of a Bogoliubov mode of the appropriate wavelength to seed modulational instability from the bosonic number distribution function

$$n(E) = \frac{1}{\exp(E/k_B T) + 1}. \quad (31)$$

Using the numbers from Sec. III, one obtains $T \simeq 0.14\mu\text{K}$ and $E_{\text{mg}}^{\text{bog}}/k_B \simeq 0.23\mu\text{K}$, so that $n(E_{\text{mg}}^{\text{bog}}) \simeq 0.17$. Thus noise caused by Bogoliubov fluctuations is present with a non-negligible occupation number for the parameters we have chosen.

A time scale for the growth of seeding fluctuations can be estimated as

$$t_{\text{noise}} \simeq 1/\gamma_{\text{mg}} = \frac{1}{2\omega_\rho|a|n_{1\text{D}}}. \quad (32)$$

This appears to be smaller by a factor of π^2 than t_{fringe} . However, given the qualitative nature of the two estimates, and the fact that they have the same parameter dependence, it is not possible to state that noise definitively dominates over the fringe mechanism. To test this, we performed additional simulations with thermally distributed and various other realizations of noise in the initial condition. These simulations show that the final

result is essentially the same as that shown in Figs. 3 and 1: 11 solitons result rather than 13, with formation first in the regions of higher density and then lower, in contrast to the case of fringes alone. Figure (4) illustrates an example of the early time evolution of the density. Solitons begin to form at $t \simeq 30$ ms, in contrast to Fig. 1, where fringes appear to self-focus at $t \simeq 40$ ms. We conclude that the two mechanisms do indeed coexist.

Noise was added into the simulations in the following manner. Because the longitudinal and transverse degrees of freedom are represented differently in the Laguerre DVR cylindrically symmetric algorithm we used, and most of the grid is not occupied in the initial state, one generates a great deal of high energy and high frequency oscillations with usual noise schemes, such as adding a small random number to the wavefunction or its Fourier transform. The fluctuations that would seed modulational instability are of long wavelength. Therefore, starting from the wavefunction on the grid in position space an FFT was implemented in the longitudinal direction. Then the wavefunction was multiplied at each point by $1 + nr$, where r was a random number between -0.5 and 0.5 and n was the noise level. In Fig. 4, $r = 0.1$ was used. In the transverse direction, the noise was added on only half the grid closest to the center. Finally, in order to allow the noise to “thermalize” as much as possible, the wavefunction was propagated in real time for positive scattering length, until the noise had fully distributed itself, *i.e.*, for times much greater than $2\pi/|\omega_z|$. This was intended to represent, qualitatively, a semi-classical approximation to a thermal distribution [26, 27] of Bogoliubov modes. Figure 4 then follows the real time evolution starting with this initial wavefunction after the scattering length is turned negative and the trap is changed to be longitudinally repulsive. In simulations with smaller noise levels we observe a coexistence regime and crossover of both seeding mechanisms, as the growth of thermal fluctuations is significantly delayed when they are initially very small.

B. Phase decoherence time

A condensate adiabatically split into two halves on a time scale much shorter than the quantum revival time has an initially well-defined relative phase [44, 45]. Estimates for the decoherence time [46] have been made in a number of specific contexts in the literature, as for example in the two-well problem [47, 48] or for two spin states [49]. A general discussion of this issue may be found in Ref. [34]. Here, we follow the straightforward estimates made in a recent article on atom interferometers using Bose-Einstein condensates, in which the phase decoherence time was studied experimentally [50, 51].

The Schrödinger phase of each soliton may be estimated from its wavefunction, which is proportional to $\exp(-i\mu t/\hbar)$:

$$\Delta\phi = t\Delta\mu/\hbar, \quad (33)$$

where t is the decoherence time. The chemical potential may be determined from Eq. (4), *i.e.*, in the quasi-1D approximation, to be

$$\mu = \frac{1}{2}\hbar\omega_\rho \left(\frac{N}{N_s}\right)^2 \left(\frac{a}{\ell_\rho}\right)^2, \quad (34)$$

where it has been assumed that N_s solitons of equal amplitude are formed. Then, from the derivative of Eq. (34) with respect to N ,

$$\frac{\Delta\mu}{\Delta N} \simeq \frac{2\mu}{N}. \quad (35)$$

For Poissonian number fluctuations, one may take $\Delta N = \sqrt{N}$. Setting $\Delta\phi = 2\pi$, which is a measure of complete uncertainty in the relative phase and therefore decoherence, Eqs. (33) and (35) yield

$$t = \frac{\pi\hbar\sqrt{N}}{|\mu|}. \quad (36)$$

Substituting Eq. (34) into Eq. (36),

$$t \simeq 2 \left(\frac{N_s}{N}\right)^2 \sqrt{N} \left(\frac{\ell_\rho}{a}\right)^2 \frac{1}{\omega_\rho}. \quad (37)$$

We note that, in contrast to a repulsive condensate in Thomas-Fermi limit, for which the decoherence time $t \propto N^{1/10}$, in the case of solitonic pulses formed by modulational instability $t \propto N^{-3/2}$. However, unlike in the repulsive case, the number of atoms is limited by the collapse conditions of Secs. IV A and IV B. For the parameters of Sec. III, the phase decoherence time may be calculated to be about 540 ms, so that the solitonic pulses shown in the figures are expected to be coherent over the evolution period depicted.

VI. DISCUSSION OF SIMULATIONS: NUMBER OF SOLITONS AND REFINED STABILITY CONDITIONS

In experiments, a good model of the initial state of the condensate when the scattering length is changed from positive to negative is a longitudinal Thomas-Fermi density profile [17]. In the following, explicit estimates for the number of solitons generated by such a profile and criteria to avoid collapse, in terms of the parameters of a possible experiment, is compared to the more idealized situation discussed in Sec. IV.

Under the condition that a suitable seed for the modulational instability is provided, one can estimate the number of solitons generated for an initially homogeneous profile along the z direction of length L by

$$N_s^{\text{hom}} \sim \frac{L}{2\pi\xi} = \sqrt{\frac{N|a|L}{\pi\ell_\rho^2}}, \quad (38)$$

where the modulational instability is assumed to take place at the wavelength of maximum growth given by Eq. (17).

The 2D collapse criterion for the initial state (3) can be refined by demanding that the solitons formed by modulational instability are themselves stable against 3D collapse and satisfy Eq. (5). For simplicity, it is assumed that the initial condensate is split up into N_s solitons of equal amplitude. As seen from the numerical simulations of Secs. III and V A, this is not strictly true, but it serves as a useful order of magnitude estimate. For the homogeneous initial profile, one finds from Eq. (38)

$$8\pi|a|N/L < \frac{8}{\pi}(\eta_c^{3D})^2 = 1.0 \dots \quad (39)$$

This estimate assumes a quasi-1D initial state, where the transverse trapping is tight, so that $|a| \ll \ell_\rho \ll \xi$. Note that under these conditions the transverse oscillator length ℓ_ρ does not enter the collapse criteria for homogeneous initial density profiles.

In the case of an inhomogeneous initial density profile the above estimates can be generalized by assuming that the length scale of $2\pi\xi$ for the modulational instability is still valid locally. The number of solitons can thus be estimated as

$$N_s = \int \frac{dz}{2\pi\xi(z)}. \quad (40)$$

For the Thomas-Fermi density profile of Eq. 26, one obtains

$$N_s^{\text{TF}} = \frac{1}{2} \left(\frac{3N|a|\ell_z}{\ell_\rho^2} \right)^{\frac{2}{3}}. \quad (41)$$

Similarly, one can derive a collapse criterion for the Thomas-Fermi case. The aspect ratio of the trap enters explicitly, and the criterion to avoid collapse is given by

$$\frac{|a|N}{\ell_z} < \frac{(\eta_c^{3D})^3}{576} \frac{\ell_z}{\ell_\rho} \approx 0.0347 \frac{\ell_z}{\ell_\rho}. \quad (42)$$

These estimates restrict the number of particles for a given scattering length that can be used in a particular trap geometry. Combining the above results, one finds an upper bound for the number of solitons that can be generated from a given trap geometry used for preparing the initial state. In the case of a rectangular initial state, or homogeneous case, one obtains

$$N_s^{\text{hom}} < 0.0635 \frac{L}{\ell_\rho}. \quad (43)$$

For a condensate initially described by a Thomas-Fermi profile one finds

$$N_s^{\text{TF}} < 0.055 \left(\frac{\ell_z}{\ell_\rho} \right)^2. \quad (44)$$

The bounds (43) and (44) were based on the 3D collapse criterion of Eq. (5). A similar analysis based on the 2D

criterion (3) for the initial wavefunction yields the same scaling but a prefactor which is an order of magnitude larger, *i.e.*, a less stringent constraint.

One may now compare these refined estimates to the simulations of Secs. III and IV D. First, the choice of $-aN/\ell_{z0}$ was taken to be about one order of magnitude smaller than the upper limit given by the criteria to avoid collapse, according to Eq. (42). Secondly, Eq. (41) predicts an upper bound on the number of solitons to be $N_s \approx 13.3$; in the simulations, between 11 and 14 solitons were observed, depending on the noise level. Thirdly, all forms of collapse have been successfully avoided, including soliton-soliton interactions which might lead to secondary collapse.

Many other parameter regimes were studied numerically. It was found that, for a rectangular initial profile and no noise, as was studied analytically in Ref. [24], increasing the strength of the nonlinearity to the critical value of $\eta_{\text{hom}} = 1$ (see Eq. (43) below) brought about immediate collapse at the *borders* of the condensate. That is, the first soliton formed collapsed. An order of magnitude decrease in η_{hom} to 0.1 led to delayed collapse which occurred after all solitons had been formed, while for $\eta_{\text{hom}} = 0.01$ no collapse occurred. Note that a rectangular initial density profile may be created by optically induced potentials which form end-caps [52], as were used in the experiment of Ref. [19].

VII. CONCLUSION

We have shown both numerically and analytically that a pulsed atomic soliton laser is viable. In particular, the figures illustrate the evolution of such an atom laser with a set of realistic parameters that could be realized in straightforward adaptations of existing BEC apparatuses [18, 19]. It was shown that all phenomena leading to instability, namely, two-dimensional primary collapse, three-dimensional primary collapse, explosion of individual solitonic pulses brought about by the longitudinally expulsive harmonic trapping potential, and secondary collapse caused by soliton-soliton interaction, could be avoided by the proper choice of parameters. Typical parameters were 10^4 particles, a final scattering length of $a \sim -3a_0$, and trapping frequencies on the order of $2\pi \times 2.2$ kHz by $2\pi \times 2.2$ kHz by $2\pi i \times 2.5$ Hz. After formation via modulational instability seeded by a combination of self-interference of the condensate order parameter and noise due to the presence of Bogoliubov quasiparticles and fluctuations in the trapping potential, propagating solitonic pulses self-cool to $T = 0$ on a time scale of $1/|\omega_z|$ through the emission of a fraction of a percent of the total number of particles [15, 16].

In most previous work on attractive Bose-Einstein condensates, regimes or cycles of runaway instability were explored [53, 54]. Even in the cases where a stable final state was produced, as for example in Refs. [18, 19], the majority of the atoms were lost to collapse. In con-

trast, we have here suggested a way to avoid collapse entirely and take advantage of the instabilities inherent in switching the interactions in a BEC from repulsive to attractive to produce a useful device: namely, a pulsed atomic soliton laser.

We acknowledge useful discussions with Jinx Cooper, Simon Gardiner, and Murray Holland, and thank H.-

D. Meyer for a preprint of Ref. [28] prior to publication. L. D. Carr gratefully acknowledges the support of the National Science Foundation via grant no. mps-drf 0104447 and the U.S. Department of Energy, Office of Basic Energy Sciences via the Chemical Sciences, Geosciences and Biosciences Division.

-
- [1] A. Hasegawa, *Optical Solitons in Fibers* (Springer-Verlag, New York, 1990).
- [2] P. G. Drazin and R. S. Johnson, *Solitons: an Introduction* (Cambridge Univ. Press, Cambridge, 1989).
- [3] G. P. Agrawal, *Nonlinear Fiber Optics*, 2nd ed. (Academic Press, San Diego, 1995).
- [4] Y. S. Kivshar, *Physics Reports* **298**, 81 (1998).
- [5] C. Sulem and P. L. Sulem, *Nonlinear Schrödinger Equations: Self-focusing Instability and Wave Collapse* (Springer-Verlag, New York, 1999).
- [6] M. O. Mewes, M. R. Andrews, D. M. Kurn, D. S. Durfee, C. G. Townsend, and W. Ketterle, *Phys. Rev. Lett.* **78**, 582 (1997).
- [7] E. W. Hagley, L. Deng, M. Kozuma, J. Wen, K. Helmenstein, S. L. Rolston, and W. D. Phillips, *Science* **283**, 1706 (1999).
- [8] B. P. Anderson and M. A. Kasevich, *Science* **282**, 1686 (1998).
- [9] I. Bloch, T. W. Hänsch, and T. Esslinger, *Phys. Rev. Lett.* **82**, 3008 (2000).
- [10] A. E. Leanhardt, Y. Shin, A. P. Chikkatur, D. Kielpinski, W. Ketterle, and D. E. Pritchard, *Phys. Rev. Lett.* **90**, 100404 (2003).
- [11] H. Ott, J. Fortagh, G. Schlotterbeck, A. Grossmann, and C. Zimmermann, *Phys. Rev. Lett.* **87**, 230401 (2001).
- [12] W. Hänsel, P. Hommelhoff, T. W. Hänsch, and J. Reichel, *Nature* **413**, 498 (2001).
- [13] M. A. Kasevich, *Science* **298**, 1363 (2002).
- [14] J. A. Sauer, M. D. Barrett, and M. S. Chapman, *Phys. Rev. Lett.* **87**, 270401 (2001).
- [15] J. Satsuma and N. Yajima, *Prog. of Theor. Phys. (Suppl.)* **55**, 284 (1974).
- [16] L. D. Carr and Y. Castin, *Phys. Rev. A* **66**, 063602 (2002).
- [17] F. Dalfovo, S. Giorgini, L. P. Pitaevskii, and S. Stringari, *Rev. Mod. Phys.* **71**, 463 (1999).
- [18] L. Khaykovich, F. Schreck, F. Ferrari, T. Bourdel, J. Cubizolles, L. D. Carr, Y. Castin, and C. Salomon, *Science* **296**, 1290 (2002).
- [19] K. E. Strecker, G. B. Partridge, A. G. Truscott, and R. G. Hulet, *Nature* **417**, 150 (2002).
- [20] P. A. Ruprecht, M. J. Holland, K. Burnett, and M. Edwards, *Phys. Rev. A* **51**, 4704 (1995).
- [21] J. M. Vogels, C. C. Tsai, R. S. Freeland, S. J. J. M. F. Kokkelmans, B. J. Verhaar, and D. J. Heinzen, *Phys. Rev. A* **56**, R1067 (1997).
- [22] S. Inouye, M. R. Andrews, J. Stenger, H.-J. Miesner, D. M. Stamper-Kurn, and W. Ketterle, *Nature* **392**, 151 (1998).
- [23] F. K. Abdullaev, J. G. Caputo, R. A. Kraenkel, and B. A. Malomed, *Phys. Rev. A* **67**, 013605 (2003).
- [24] L. D. Carr and J. Brand, *Phys. Rev. Lett.* **92**, 040401 (2004).
- [25] A. Hasegawa and W. F. Brinkman, *IEEE J. Quantum Electron.* **16**, 694 (1980).
- [26] A. Sinatra, C. Lobo, and Y. Castin, *Phys. Rev. Lett.* **87**, 210404 (2001).
- [27] M. J. Davis, S. A. Morgan, and K. Burnett, *Phys. Rev. A* **66**, 053618 (2002).
- [28] For representing the transverse degree of freedom a Laguerre DVR was used as described in C. W. McCurdy, W. A. Isaacs, H.-D. Meyer, and T. N. Rescigno, *Phys. Rev. A* **67**, 042708 (2003).
- [29] M. I. Weinstein, *Comm. Math. Phys.* **87**, 567 (1983).
- [30] L. P. Pitaevskii, *Phys. Lett. A* **221**, 14 (1996).
- [31] M. Olshanii, *Phys. Rev. Lett.* **81**, 938 (1998).
- [32] A. Gammal, T. Frederico, and L. Tomio, *Phys. Rev. A* **64**, 055602 (2001).
- [33] H. K. Ng, K. D. Moll, and A. L. Gaeta, 2004, submitted to *Phys. Rev. A*.
- [34] C. Cohen-Tannoudji, *Cours de physique atomique et moléculaire*, <http://www.lkb.ens.fr/~cct/cours/>, 1999.
- [35] H. Michinel, V. Pérez-García, and R. de la Fuente, *Phys. Rev. A* **60**, 1513 (1999).
- [36] J. P. Gordon and H. A. Haus, *Opt. Lett.* **11**, 665 (1986).
- [37] P. V. Elyutin, A. V. Buryak, V. V. Gubernov, R. A. Sammut, and I. N. Towers, *Phys. Rev. E* **64**, 016607 (2002).
- [38] U. A. Khawaja, H. T. C. Stoof, R. G. Hulet, K. E. Strecker, and G. B. Partridge, *Phys. Rev. Lett.* **89**, 200404 (2002).
- [39] L. D. Carr, M. A. Leung, and W. P. Reinhardt, *J. Phys. B: At. Mol. Opt. Phys.* **33**, 3983 (2000).
- [40] J. Fortagh, H. Ott, S. Kraft, A. Gunther, and C. Zimmermann, *Phys. Rev. A* **66**, 041604 (2002).
- [41] J. J. García-Ripoll, V. M. Pérez-García, and V. Vekslerchik, *Phys. Rev. E* **64**, 056602 (2001).
- [42] N. N. Akhmediev, V. I. Korneev, and R. F. Nabiev, *Opt. Lett.* **17**, 393 (1992).
- [43] A. M. Kamchatnov, A. Gammal, F. K. Abdullaev, and R. A. Kraenkel, *Phys. Lett. A* **319**, 406 (2003).
- [44] E. M. Wright, D. F. Walls, and J. C. Garrison, *Phys. Rev. Lett.* **77**, 2158 (1996).
- [45] C. Menotti, J. R. Anglin, J. I. Cirac, and P. Zoller, *Phys. Rev. A* **63**, 023601 (2001).
- [46] M. Lewenstein and L. You, *Phys. Rev. Lett.* **77**, 3489 (1996).
- [47] J. Javanainen and M. Wilkens, *Phys. Rev. Lett.* **78**, 4675 (1997).
- [48] Y. Castin and J. Dalibard, *Phys. Rev. A* **55**, 4330 (1997).
- [49] A. Sinatra and Y. Castin, *Eur. Phys. J. D* **9**, 319 (2004).
- [50] Y. Shin, M. Saba, T. A. Pasquini, W. Ketterle, D. E. Pritchard, and A. E. Leanhardt, *Phys. Rev. Lett.* **92**,

- 050405 (2004).
- [51] 2004, private communication, A. E. Leanhardt, MIT.
- [52] K. Bongs, S. Burger, S. Dettmer, D. Hellweg, J. Arlt, W. Ertmer, and K. Sengstock, *Phys. Rev. A* **63**, 031602 (2001), e-print cond-mat/0007381.
- [53] C. A. Sackett, H. T. C. Stoof, and R. G. Hulet, *Phys. Rev. Lett.* **80**, 2031 (1998).
- [54] E. A. Donley, N. R. Claussen, S. L. Cornish, J. L. Roberts, E. A. Cornell, and C. E. Wieman, *Nature* **412**, 295 (2001).